

High-Efficiency Spray-Coated Perovskite Solar Cells Utilizing Vacuum-Assisted Solution Processing

James E. Bishop,[†] Joel A. Smith,[†] Claire Greenland,[†] Vikas Kumar,^{‡,ID} Naoum Vaenas,[†] Onkar S. Game,^{‡,ID} Thomas J. Routledge,^{‡,ID} Michael Wong-Stringer,^{‡,ID} Cornelia Rodenburg,[‡] and David G. Lidzey^{*,†,ID}

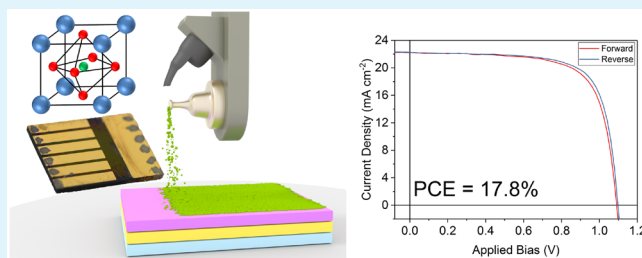
[†]Department of Physics & Astronomy, University of Sheffield, Hicks Building, Hounsfield Road, Sheffield S3 7RH, United Kingdom

[‡]Department of Materials Science & Engineering, University of Sheffield, Mappin Street, Sheffield S1 3JD, United Kingdom

S Supporting Information

ABSTRACT: We use ultrasonic spray-coating to fabricate cesium-containing triple-cation perovskite solar cells with a power-conversion efficiency of up to 17.8%. Our fabrication route involves a brief exposure of the partially wet spray-cast films to a low vacuum, a process that is used to control film crystallization. We show that films that are not vacuum-exposed are relatively rough and inhomogeneous, while vacuum-exposed films are smooth and consist of small and densely packed perovskite crystals. The process techniques developed here represent a step toward a scalable and industrially compatible manufacturing process capable of creating stable and high-performance perovskite solar cells.

KEYWORDS: perovskite solar cell, ultrasonic spray-coating, triple-cation perovskite, low hysteresis, thin film



Metal-halide perovskites are high-performance semiconductor materials that have received significant attention due to their applications in photovoltaic (PV) devices. Although the initial power-conversion efficiencies (PCEs) of perovskite PV devices were low (3.8% in 2009),¹ they have increased rapidly as a result of worldwide research effort, with the best single junction devices now having an efficiency in excess of 23% PCE.² Perovskites combine many properties that make them effective photovoltaic materials, including efficient light absorption, tunable band gap, high charge-carrier mobility, and low non-radiative recombination rates.^{3,4} Importantly, perovskite films can be formed from solution at low temperature, a useful property for the mass production of cheap, efficient solar cells using a variety of scalable deposition techniques such as slot-die coating,⁵ ink-jet printing,⁶ blade coating,⁷ and spray-coating.⁸

For perovskite PV devices to be manufacturable at high volume, it is necessary to develop practical processes that enable the fabrication of high quality, uniform thin films. Among the techniques that are currently being explored to fabricate perovskite PV devices, spray-coating has emerged as an industrially compatible process that can coat large areas at speed. Ultrasonic spray-coating was first used to deposit a $\text{CH}_3\text{NH}_3\text{I}/\text{PbCl}_2$ precursor ink, which was then used to fabricate PV devices having a maximum PCE of 11%.⁸ A number of groups have subsequently explored spray-coating to deposit perovskite materials, with a range of techniques explored. Notably, Das et al. created spray-cast $\text{CH}_3\text{NH}_3\text{PbI}_{3-x}\text{Cl}_x$ PV devices using a compact TiO_2 and

spiro-OMeTAD electron- and hole-transport layers, with an efficiency of 13% being demonstrated.⁹ Tait et al. further improved device efficiency to 15.7% by spray-casting PV devices based on a lead acetate/ PbCl_2 precursor.¹⁰ By separately spray-coating PbI_2 and methylammonium iodide (MAI) in a two-step process, Huang et al. improved device efficiency to 16.03%.¹¹ Recent work by Heo et al.¹² explored a process in which a substrate held at 120 °C was continually spray-coated with a DMF/GBL solution containing $\text{CH}_3\text{NH}_3\text{PbI}_{3-x}\text{Cl}_x$ for 2 min. By balancing incoming and outgoing solvent fluxes (with the outgoing flux controlled via solvent composition), they created a solvent-rich layer in which the growth of large perovskite grains was encouraged, forming highly uniform perovskite films.¹² Such films were then combined with other spin-cast charge-extraction layers to create a PV device with 18.3% PCE. While such efficiencies are very impressive, there are questions about whether such a slow deposition process would be commercially scalable. Second, we note that the $\text{CH}_3\text{NH}_3\text{PbI}_{3-x}\text{Cl}_x$ perovskite is thermally unstable above 85 °C due to the low energy required to liberate organic decomposition products from the perovskite crystal lattice,^{13,14} a feature that might limit its possible applications.

To circumvent this problem, researchers have increasingly turned to the use of mixed cation and halide systems. Here,

Received: August 30, 2018

Accepted: November 9, 2018

Published: November 9, 2018

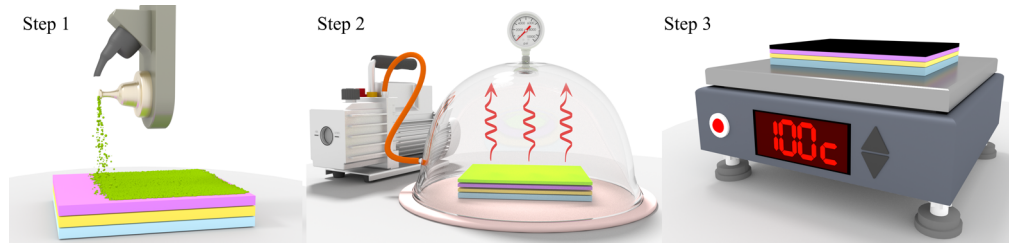


Figure 1. Schematic illustration of the spray-deposition and VASP treatment process used to fabricate high-quality perovskite films. In step 1, the spray-head moves across the surface depositing the precursor ink, which then forms into a wet film. In step 2, the wet film is exposed to a partial vacuum for 5 min to drive out the DMF from the film, forming a partially crystallized layer. In step 3, the semicrystallized perovskite film is annealed at 100 °C to form the perovskite phase.

formamidinium[$\text{HC}(\text{NH}_2)_2$] (FA) was first introduced into a methylammonium-based perovskite to reduce the semiconductor band gap and thereby increase optical absorption at longer wavelengths.¹⁵ It was then found that the photoactive black phase of FAPbI_3 ¹⁶ could be stabilized by combining MAPbBr_3 with FAPbI_3 . Further improvements in material properties then resulted from the addition of cesium to the perovskite, creating high-performance and stable “triple-cation” devices with PCEs of up to 21.1%.¹⁷ While this material system currently represents the state of the art for perovskite semiconductors, triple-cation perovskites have not yet been deposited by spray-coating.

In this article, we demonstrate for the first time the spray-deposition of triple-cation perovskite layers, which we then use to produce cells with PCEs up to 17.8%. Importantly, we utilize a vacuum flash assisted solution-processing (VASP) method¹⁸ to control the crystallization of the wet precursor film, with this technique allowing us to spray-coat highly specular perovskite films of comparable quality with those produced via spin-coating. This combination of advanced materials selection, scalable-deposition processes, and control over crystallization processes are likely be key ingredients in a spray-based manufacture process.

The perovskite precursor inks from which we have fabricated PV devices were created from a mixture of cesium iodide, formamidinium iodide, lead iodide, methylammonium bromide, and lead bromide dissolved in a mixture of dimethylformamide (DMF) and dimethyl sulfoxide (DMSO) at a 4:1 ratio. The powders were mixed stoichiometrically, such that the final perovskite precursor had the composition $\text{CsI}_{0.05}((\text{FAPbI}_3)_{0.85}(\text{MAPbBr}_3)_{0.15})_{0.95}$. A detailed process recipe and further experimental details are given in the Supporting Information.

Thin films were spray-cast using a Sonotek ExactaCoat system fitted with an “Impact” ultrasonic nozzle, with the system located inside a nitrogen-filled glovebox. Our deposition process is summarized schematically in Figure 1. The ultrasonic spray-coating process is based on a piezoelectric nozzle that is resonated at a kilohertz frequency. A solution of interest is then fed through the nozzle, with shear forces created by the oscillation causing the solution to break into a mist of micron-sized droplets. A carrier gas (in this case, nitrogen) is then used to guide the droplets to the surface. The key advantage of ultrasonic spray-coating over traditional air-brush techniques is that a highly uniform size distribution of droplets can be generated. This can, in principle, lead to the formation of more-uniform surface coatings and, hence, better-quality films.^{8,19,20}

In the experiments described, the ultrasonic spray-head was mounted onto a motorized gantry, with the spray-head moving across the substrate and coating it in a single pass that took a few seconds. This process reproduces the action of a R2R production line, in which a substrate moves continuously through the system (here, corresponding to a coating velocity of 50 mm s⁻¹).

We have found through careful optimization that uniform perovskite precursor films can be created by spray-coating the precursor ink onto a substrate held at 40 °C at a flow rate of 1 mL min⁻¹. Coating was performed at a spray-head velocity of 50 mm s⁻¹ with a head height of 10 cm above the substrate, with a shaping gas pressure of 3 psi and an ultrasonic nozzle power of 2 W. This produces a spray pattern 3 cm wide that we use to coat our substrates in a single pass. After 30 s, droplets were observed to have merged into a uniform wet film. As we describe below, it is critical that this wet film is exposed to a partial (low) vacuum. Following this vacuum-exposure process, films were annealed at 100 °C for 30 min to remove any remaining DMSO and convert the film into a smooth (root-mean-square roughness of 22 nm) black perovskite film (see Figure S1).

To create PV devices, we have used the architecture of indium tin oxide (ITO)/np-SnO₂/perovskite/spiro-OMeTAD/Au. Here, the nanoparticle (np) SnO₂ film²¹ was deposited by spin-coating a commercially available np-SnO₂ solution onto the ITO, which was then annealed at 150 °C for 30 min. To complete the device, a layer of doped spiro-OMeTAD was spin-cast onto the perovskite layer, followed by a gold top contact deposited by thermal evaporation through a shadow-mask, forming a series of 2 mm × 2 mm electrode-contacts. Devices were then tested via current–voltage (JV) measurements following exposure (through a 2.6 mm² aperture mask) to light from an AM 1.5 calibrated solar simulator. To explore film morphology and crystallinity, we performed scanning electron microscopy and thin-film X-ray diffraction. Device homogeneity was also characterized using laser-beam-induced current (LBIC) measurements. Here, light from a 635 nm laser was focused onto the cell and then raster-scanned in two dimensions while the photocurrent generated was recorded.

We have also performed time-resolved photoluminescence (TRPL) mapping of spray-cast films deposited on glass. Here, a pulsed laser was focused onto the film using a microscope lens, with the laser spot raster-scanned across the surface. The PL emission that was generated was collected using the same microscope lens. A time-correlated single photon-counting technique was then used to produce a TRPL decay curve at each location. These decay curves were fitted with a

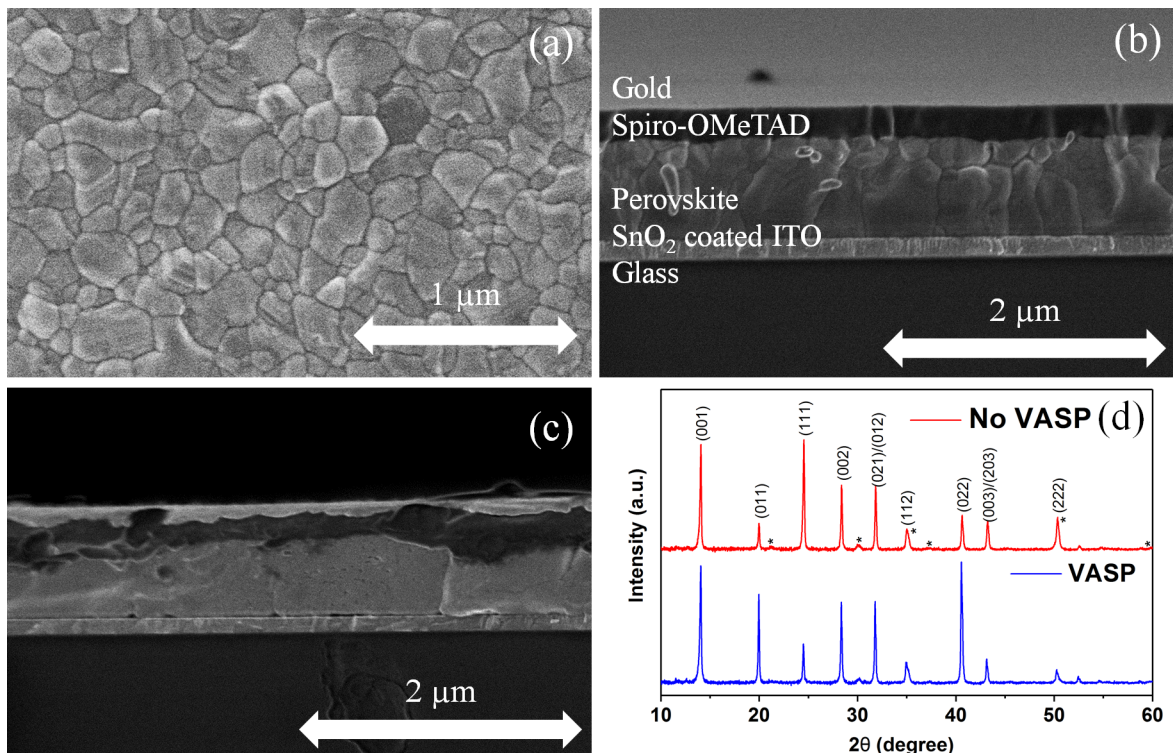


Figure 2. (a) SEM surface image of a spray-cast VASP treated triple-cation perovskite film. (b, c) A cross-sectional SEM of a completed device containing a spray-cast triple-cation perovskite layer. Here, the perovskite film shown in panel b was exposed to a vacuum, while the film shown in panel c was thermally annealed. Panel d shows the results of thin film XRD measurements on VASP-treated and untreated films. The asterisks indicate background peaks from the substrate.

biexponential function, allowing us to build an image of the bimolecular recombination lifetime.

Perovskite films are polycrystalline in nature, and controlling the morphology of such films often presents a challenge because the size, shape, and interconnectedness of the crystal grains is highly dependent on processing conditions. When triple-cation perovskite precursor films are deposited by spin-coating, it is common to utilize a so-called “anti-solvent quenching technique”, in which the precursor film is exposed to either chlorobenzene, toluene, or some other nonpolar solvent.²² This exposure rapidly drives DMF out of the film,²³ with the remaining DMSO forming a crystalline intermediary phase with the perovskite constituents.²⁴ Subsequent annealing of the film removes the DMSO, thereby forming a high-quality perovskite layer. In our experiments, we have found that it is relatively straightforward to create a uniform triple-cation perovskite precursor film by spray-coating; however, the conversion of such a film into an optically dense, specular perovskite film is difficult. Simply annealing the unconverted precursor-film results in perovskite-films that are characterized by poor surface coverage and a high degree of roughness (100 nm). This appears to occur because there are insufficient nucleation sites for the crystallization of the perovskite phase,²⁵ and as the substrate is heated, the rate of crystal growth suppresses the formation of further nucleation sites. This results in a film characterized by large crystallites having a lateral size of tens of microns^{8,26} rather than a uniform film composed of small, densely packed crystallites (see Figures S2 and S3). We have found that PV devices based on triple-cation films created via a regular spray-coating process followed by thermal annealing are characterized by a low open circuit

voltage and thus relatively low PCEs of around 10% (see Figure S4).

We note that Ulicna et al. have recently demonstrated high-efficiency (17.3%) $\text{CH}_3\text{NH}_3\text{PbI}_{3-x}\text{Cl}_x$ spray-cast devices created by dipping a precursor film in diethyl ether to rapidly extract DMF from the film.²⁷ We have tried to replicate such an anti-solvent quench process, with both the perovskite precursor and the antisolvent (chlorobenzene) delivered to the surface via spray-coating. Unfortunately, this has proven to be an ineffective means of inducing the intermediate perovskite–DMSO phase. We also note that the scalability of this process is suboptimal because it requires the use and recovery of significant quantities of solvent.

To address this issue, we have explored a vacuum-based solvent extraction process developed by Li et al.¹⁸ Here, it was shown that by exposing a freshly spin-cast FA and MA mixed cation/iodide–bromide mixed anion precursor film to a low vacuum, it was possible to form a DMSO intermediary phase. Upon the annealing of such vacuum-treated films, high-quality, fully crystalline perovskite layers were formed that were used to create high-efficiency (20.5%) PV devices.

We have applied this technique to freshly spray-cast triple-cation perovskite precursor films, with films placed in a glovebox antechamber (reaching a final pressure of 0.8 mbar) for a period of 5 min immediately after deposition. A scanning electron microscopy (SEM) image of the perovskite film surface and a device cross-section is shown in panels a and b of Figure 2, respectively. Here, it can be seen that the film is composed of tightly packed grains with an average lateral size of around 200 nm. Figure 2c shows a cross-section of an otherwise identical spray-cast device that was fabricated without vacuum exposure. Here, it is evident that the

perovskite layer is highly nonuniform, with significant thickness variations occurring over micron length scales and numerous voids visible throughout the layer.

To compare the crystallinity of VASP treated and annealed-only triple-cation perovskite films, we used X-ray diffraction (XRD), shown in Figure 2d. Samples were scanned across a broad 2θ range, and peaks were identified as associated with the room-temperature cubic perovskite structure (space group $Pm3m$).²⁸ Comparing the scattering patterns of the two films, we find that there is significantly lower scattering intensity from the (011) plane in the untreated film; however, scattering from the (111) plane is greatly increased, with scattering intensity from both the (002) and the (021) and (012) peaks being reduced. Notably, there is no evidence of remnant solvent complexes or other precursor phases, which would be observed at small scattering angles in the region $2\theta < 14^\circ$.²² This result suggests that the material formed in both cases is a cubic perovskite, but the different crystallization routes clearly lead to a change in the crystal orientation of the resultant film. This difference in crystallographic orientation may impact the device performance due to different charge transport characteristics and interface behavior. However, the improved nanoscale morphology, controlled nucleation, and overall better film quality achieved via the VASP treatment route are anticipated to play a dominant role in delivering high device performance.

We have utilized this vacuum-treatment step to make a series of photovoltaic devices. A current–voltage (J – V) curve of a champion device is shown in Figure 3a. Here, upon reverse sweeping, we obtained a device PCE of 17.8%, a value that compares favorably to the current highest efficiency spray-cast devices reported by Heo et al. that had an efficiency of 18.3%.¹² It is clear that the devices have only minimal hysteresis, a fact that we attribute to the use of SnO_2 nanoparticles, which have more-favorable band alignment to triple-cation perovskite than the more widely used TiO_2 .^{21,29}

In Table 1, we tabulate the average performance metrics of 18 2.6 mm^2 spray-cast cells together with champion cell metrics. While this is a relatively small sample size, the low hysteresis and small standard deviation suggests that our process is highly reproducible. Indeed, the J_{SC} and V_{OC} values are consistently high, with variations in efficiency occurring as a result of a scatter in device fill factor (FF). The origin of this scatter in FF is currently not understood. We have determined the wavelength-dependent external quantum efficiency (EQE) of a representative cell, as shown in Figure 3b. Here, the integrated J_{SC} value of 20.3 mA cm^{-2} is within 6% of the average value reported in Table 1 (21.4 mA cm^{-2}). Unfortunately our EQE system cannot measure spectral response below 380 nm, and thus, the integrated J_{SC} is likely to be a slight underestimate of its actual value. We have also fabricated larger area devices (active area of 16 mm^2) that have similar device performance to small area devices (see Figure 3c). A stabilized measurement recorded from such a device (15.4%) is shown in Figure S5.

To explore the homogeneity of the device photocurrent across the active area, we have performed LBIC measurements on spray-cast devices fabricated either with or without the additional vacuum-exposure step. Typical images are shown in Figure 4. Panel a shows an LBIC image of a device in which the perovskite precursor material had not undergone vacuum crystallization. Here, it can be seen that there is a significant variation in the photocurrent generation over length scales of around $100 \mu\text{m}$. Panel b shows an image of a comparable

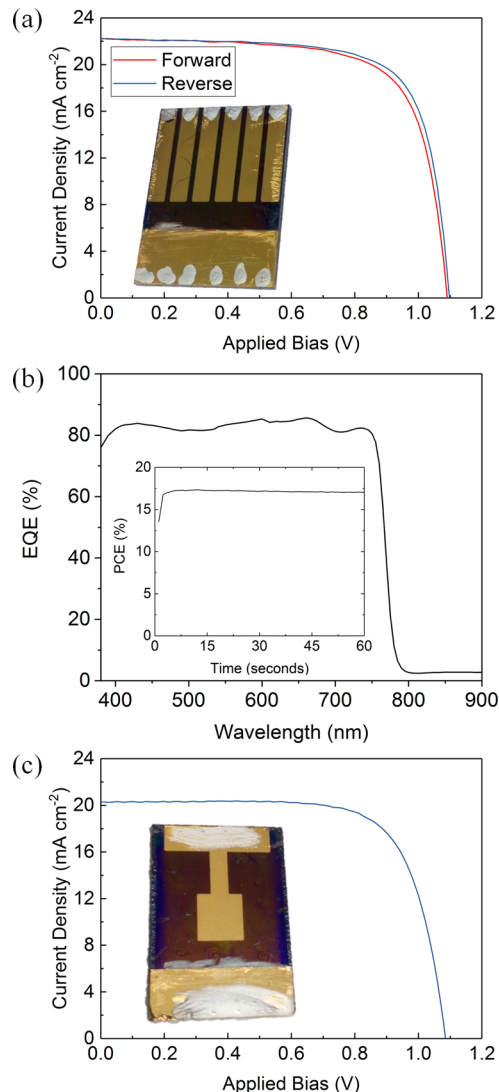


Figure 3. (a) Current–voltage characteristics for the champion spray-cast triple-cation perovskite solar cell with a reverse scan efficiency of 17.8%. The inset shows a photograph of the device. (b) An EQE spectrum recorded from a representative spray-cast perovskite cell ($J_{\text{SC}}: 21.4 \text{ mA cm}^{-2}$) corresponding to an integrated current of 20.3 mA cm^{-2} . The inset shows output power of the champion device held at a fixed voltage close to the maximum power point (920 mV) recorded over 60 s, indicating a stabilized power output of 17%. (c) The current voltage characteristics of a larger-area device with a reverse-scan efficiency of 16%. The inset shows a photograph of the device.

device that was fabricated using vacuum exposure; here, the generated photocurrent appears significantly more uniform, apart from a small number of “cold spots” that again have an average diameter of around $100 \mu\text{m}$. We anticipate that such features most likely correspond to undissolved aggregates (most likely composed of lead-based compounds) that were originally contained within the perovskite precursor solution.²⁶

To understand whether charge-carrier lifetimes differ between VASP-treated and untreated films, we have performed time-resolved photoluminescence (TRPL) mapping of films deposited on glass substrates. Figure 4c,d shows microscope images of regions from untreated and treated samples that were then selected for mapping. It is clear from these images that the VASP-treated film is significantly more uniform,

Table 1. Reverse- and Forward-Sweep Performance Metrics for 18 Spray-Cast Perovskite Solar Cells^a

scan direction	J_{SC} (mA cm ⁻²)	V_{OC} (V)	FF (%)	PCE (%)
forward	22.2 (21.4 ± 0.4)	1.09 (1.07 ± 0.01)	71 (65 ± 5)	17.3 (14.7 ± 1.4)
reverse	22.3 (21.4 ± 0.4)	1.10 (1.08 ± 0.01)	73 (65 ± 4)	17.8 (15.1 ± 1.3)

^aBold font indicates device metrics for the champion cell. Data shown in parentheses represent average device metrics and associated standard deviation.

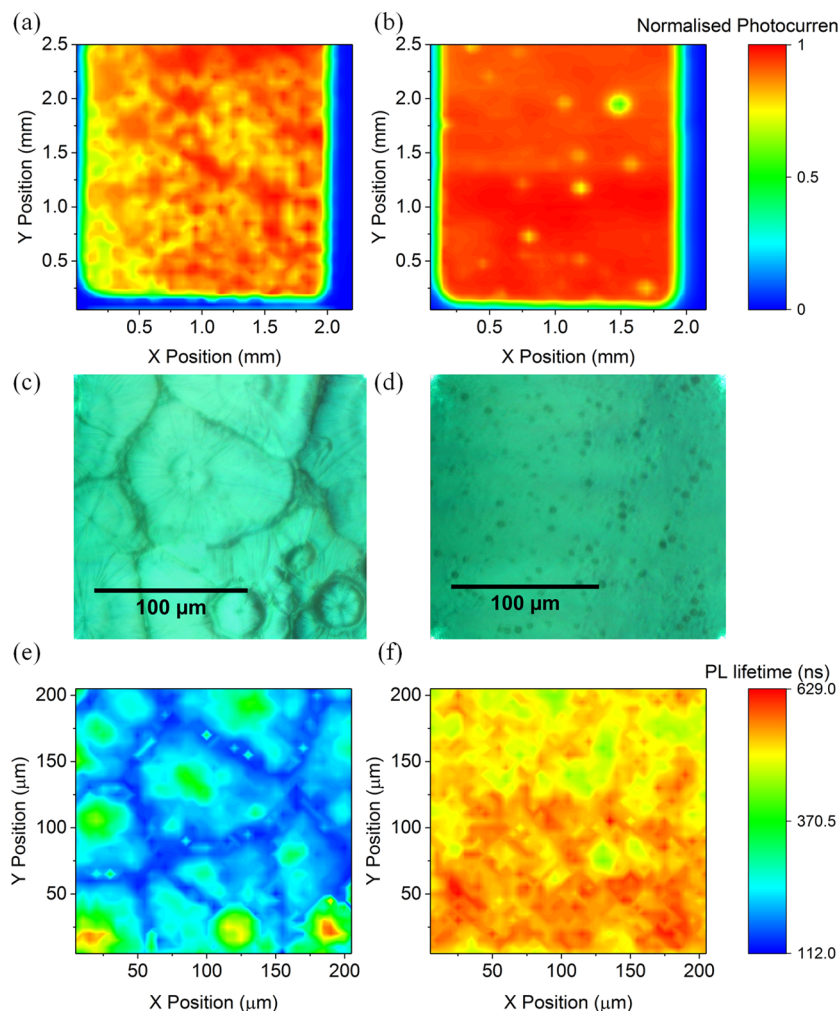


Figure 4. Laser-beam-induced current (LBIC) mapping, optical-microscope images, and time-resolved photoluminescence (TRPL) mapping of spray-cast perovskite solar cells and films. (a) An LBIC image of device that includes a perovskite layer that was thermally annealed only. (b) A comparable device in which the perovskite precursor film was treated using the additional VASP process. (c) An optical micrograph of a spray-cast film deposited on glass that had simply been annealed. (d) A film that has undergone VASP treatment. (e, f) TRPL maps of the same regions of the film shown in panels c and d.

whereas the untreated film is dominated by large “flower-like” crystallites. Figure 4e,f shows TRPL maps of the long decay lifetimes extracted from fits to the bimolecular recombination decay curves. Examples of the fits used to calculate these values are presented in Figure S6. Here, the flower-like crystallites are clearly resolved, with the emission from the edges of such features apparently having much shorter lifetimes than those recorded from their center. We speculate this is due to a higher density of non-radiative recombination centers found in these regions that occur as a result of a more-disordered macrostructure together with compositional variations that are also observed in energy-dispersive X-ray spectroscopy (see Figure S7). In contrast, the VASP-treated films are characterized by

much longer average decay lifetimes, with such decay transients having enhanced uniformity across the film surface.

In conclusion, we have demonstrated a method to fabricate triple-cation-based perovskite solar cells having a peak power conversion efficiency of 17.8% using a combination of ultrasonic spray-coating and vacuum-assisted solution processing. The device efficiencies demonstrated are comparable with the highest efficiencies reported for spray-cast perovskite devices.¹² Here the use of a relatively low vacuum both removes trapped solvent and initiates crystallization through controlled nucleation, with the films produced being of comparable quality with those produced via spin-coating. This allows us to create PV devices having enhanced photocurrent uniformity, as evidenced using photocurrent

mapping studies. Importantly, our work is the first example of the use of spray-casting to fabricate photovoltaic devices based on a triple-cation perovskite. Such perovskite materials are compatible with stable device operation over prolonged time-scales¹⁷ and have higher efficiency than those based on methylammonium lead triiodide, the current material of choice used to spray-cast PV devices.^{8–12} We anticipate that further process optimization will allow us to create spray-coated perovskite devices having efficiencies that match the state of the art. The process demonstrated uses a rapid single-pass spray technique and is thus an important step toward high-speed, high-volume perovskite PV device manufacturing. Indeed, we expect that the deposition process used here could be further accelerated by using flash-infrared annealing instead of the relatively slow thermal-annealing stage.³⁰ We emphasize that the use of vacuum-processing steps are compatible with high-volume manufacturing; for example, metallized films are routinely deposited on moving substrate films such as polyethylene terephthalate via vacuum-based physical vapor deposition.³¹ Notably, our process does not require the use of large quantities of solvent in either the initial spray-deposition step or subsequent anti-solvent quenching and is thus a step toward a more environmentally benign manufacturing process.

■ ASSOCIATED CONTENT

Supporting Information

The Supporting Information is available free of charge on the ACS Publications website at DOI: [10.1021/acsmami.8b14859](https://doi.org/10.1021/acsmami.8b14859).

Experimental details on perovskite sample preparation and additional characterization including atomic force microscopy, photoluminescence, and energy-dispersive X-ray analysis ([PDF](#))

■ AUTHOR INFORMATION

Corresponding Author

*E-mail: d.g.lidzey@sheffield.ac.uk.

ORCID

Vikas Kumar: [0000-0002-1034-2915](https://orcid.org/0000-0002-1034-2915)

Onkar S. Game: [0000-0002-5573-3602](https://orcid.org/0000-0002-5573-3602)

Thomas J. Routledge: [0000-0003-0890-113X](https://orcid.org/0000-0003-0890-113X)

Michael Wong-Stringer: [0000-0002-4364-4127](https://orcid.org/0000-0002-4364-4127)

David G. Lidzey: [0000-0002-8558-1160](https://orcid.org/0000-0002-8558-1160)

Notes

The authors declare the following competing financial interest(s): D.G.L. is co-director of a company, Ossila Limited, that sells materials and equipment for perovskite photovoltaic device research and development.

■ ACKNOWLEDGMENTS

This work was funded by the U.K. Engineering and Physical Sciences Research Council (EPSRC) via grants no. EP/M025020/1 “High resolution mapping of performance and degradation mechanisms in printable photovoltaic devices”, EPSRC grant no. EP/N008065/1 “Secondary Electron Emission - Microscopy for Organics With Reliable Engineering-Properties”, and no. EP/M014797/1 “Improved Understanding, Development and Optimization of Perovskite-based Solar Cells”. We also thank the EPSRC for PhD studentships via the University of Sheffield DTG account (J.E.B. and T.J.R.) and from the Centre for Doctoral Training in New and

Sustainable PV, EP/L01551X/1 (M.W.S., J.A.S., and C.G.). We thank Dave Coles for providing an illustration of the spray-deposition process for [Figure 1](#).

■ REFERENCES

- (1) Kojima, A.; Teshima, K.; Shirai, Y.; Miyasaka, T. Organometal Halide Perovskites as Visible-Light Sensitizers for Photovoltaic Cells. *J. Am. Chem. Soc.* **2009**, *131*, 6050–6051.
- (2) NREL. Best Research-Cell Efficiencies. <https://www.nrel.gov/pv/assets/images/efficiency-chart-20180716.jpg> (accessed August 15, 2018).
- (3) Stranks, S. D.; Eperon, G. E.; Grancini, G.; Menelaou, C.; Alcocer, M. J.; Leijtens, T.; Herz, L. M.; Petrozza, A.; Snaith, H. J. Electron-Hole Diffusion Lengths Exceeding 1 Micrometer in an Organometal Trihalide Perovskite Absorber. *Science* **2013**, *342*, 341–344.
- (4) Green, M. A.; Ho-Baillie, A.; Snaith, H. J. The Emergence of Perovskite Solar Cells. *Nat. Photonics* **2014**, *8*, S06–S14.
- (5) Schmidt, T. M.; Larsen-Olsen, T. T.; Carlé, J. E.; Angmo, D.; Krebs, F. C. Upscaling of Perovskite Solar Cells: Fully Ambient Roll Processing of Flexible Perovskite Solar Cells with Printed Back Electrodes. *Adv. Energy Mater.* **2015**, *5*, 1500569.
- (6) Li, S.-G.; Jiang, K.-J.; Su, M.-J.; Cui, X.-P.; Huang, J.-H.; Zhang, Q.-Q.; Zhou, X.-Q.; Yang, L.-M.; Song, Y.-L. Inkjet Printing of CH 3 NH 3 PbI 3 on a Mesoscopic TiO 2 Film for Highly Efficient Perovskite Solar Cells. *J. Mater. Chem. A* **2015**, *3*, 9092–9097.
- (7) Deng, Y.; Peng, E.; Shao, Y.; Xiao, Z.; Dong, Q.; Huang, J. Scalable Fabrication of Efficient Organolead Trihalide Perovskite Solar Cells with Doctor-Bladed Active Layers. *Energy Environ. Sci.* **2015**, *8*, 1544–1550.
- (8) Barrows, A. T.; Pearson, A. J.; Kwak, C. K.; Dunbar, A. D.; Buckley, A. R.; Lidzey, D. G. Efficient Planar Heterojunction Mixed-Halide Perovskite Solar Cells Deposited via Spray-Deposition. *Energy Environ. Sci.* **2014**, *7*, 2944–2950.
- (9) Das, S.; Yang, B.; Gu, G.; Joshi, P. C.; Ivanov, I. N.; Rouleau, C. M.; Aytug, T.; Geohegan, D. B.; Xiao, K. High-Performance Flexible Perovskite Solar Cells by using a Combination of Ultrasonic Spray-Coating and Low Thermal Budget Photonic Curing. *ACS Photonics* **2015**, *2*, 680–686.
- (10) Tait, J.; Manghooli, S.; Qiu, W.; Rakocevic, L.; Kootstra, L.; Jaysankar, M.; Masse de la Huerta, C. A.; Paetzold, U. W.; Gehlhaar, R.; Cheyns, D.; Heremans, P.; Poortmans, J. Rapid Composition Screening for Perovskite Photovoltaics via Concurrently Pumped Ultrasonic Spray Coating. *J. Mater. Chem. A* **2016**, *4*, 3792–3797.
- (11) Huang, H.; Shi, J.; Zhu, L.; Li, D.; Luo, Y.; Meng, Q. Two-Step Ultrasonic Spray Deposition of CH 3 NH 3 PbI 3 for Efficient and Large-Area Perovskite Solar Cell. *Nano Energy* **2016**, *27*, 352–358.
- (12) Heo, J. H.; Lee, M. H.; Jang, M. H.; Im, S. H. Highly Efficient CH 3 NH 3 PbI 3- x Cl x Mixed Halide Perovskite Solar Cells Prepared by Re-dissolution and Crystal Grain Growth via Spray Coating. *J. Mater. Chem. A* **2016**, *4*, 17636–17642.
- (13) Conings, B.; Drijkoningen, J.; Gauquelin, N.; Babayigit, A.; D'Haen, J.; D'Olieslaeger, L.; Ethirajan, A.; Verbeeck, J.; Manca, J.; Mosconi, E.; De Angelis, F.; Boyen, H.-G. Intrinsic Thermal Instability of Methylammonium Lead Trihalide Perovskite. *Adv. Energy Mater.* **2015**, *5*, 1500477.
- (14) Juarez-Perez, E. J.; Ono, L. K.; Maeda, M.; Jiang, Y.; Hawash, Z.; Qi, Y. Photodecomposition and Thermal Decomposition in Methylammonium Halide Lead Perovskites and Inferred Design Principles to Increase Photovoltaic Device Stability. *J. Mater. Chem. A* **2018**, *6*, 9604–9612.
- (15) Pellet, N.; Gao, P.; Gregori, G.; Yang, T.-Y.; Nazeeruddin, M. K.; Maier, J.; Grätzel, M. Mixed-Organic-Cation Perovskite Photovoltaics for Enhanced Solar-Light Harvesting. *Angew. Chem.* **2014**, *126*, 3215–3221.
- (16) Jeon, N. J.; Noh, J. H.; Yang, W. S.; Kim, Y. C.; Ryu, S.; Seo, J.; Seok, S. I. Compositional Engineering of Perovskite Materials for High-Performance Solar Cells. *Nature* **2015**, *517*, 476–480.

- (17) Saliba, M.; Matsui, T.; Seo, J.-Y.; Domanski, K.; Correa-Baena, J.-P.; Nazeeruddin, M. K.; Zakeeruddin, S. M.; Tress, W.; Abate, A.; Hagfeldt, A.; Grätzel, M. Cesium- Containing Triple Cation Perovskite Solar Cells: Improved Stability, Reproducibility and High Efficiency. *Energy Environ. Sci.* **2016**, *9*, 1989–1997.
- (18) Li, X.; Bi, D.; Yi, C.; Déköppet, J.-D.; Luo, J.; Zakeeruddin, S. M.; Hagfeldt, A.; Grätzel, M. A Vacuum Flash-Assisted Solution Process for High-Efficiency Large-Area Perovskite Solar Cells. *Science* **2016**, *353*, 58.
- (19) Majumder, M.; Rendall, C.; Li, M.; Behabtu, N.; Eukel, J. A.; Hauge, R. H.; Schmidt, H. K.; Pasquali, M. Insights into the Physics of Spray Coating of SWNT Films. *Chem. Eng. Sci.* **2010**, *65*, 2000–2008.
- (20) Bishop, J. E.; Routledge, T. J.; Lidzey, D. G. Advances in Spray-Cast Perovskite Solar Cells. *J. Phys. Chem. Lett.* **2018**, *9*, 1977–1984.
- (21) Jiang, Q.; Zhang, L.; Wang, H.; Yang, X.; Meng, J.; Liu, H.; Yin, Z.; Wu, J.; Zhang, X.; You, J. Enhanced Electron Extraction using SnO₂ for High-Efficiency Planar-Structure HC (NH₂)₂PbI₃-based Perovskite Solar Cells. *Nature Energy* **2017**, *2*, 16177.
- (22) Paek, S.; Schouwink, P.; Athanasopoulou, E. N.; Cho, K.; Grancini, G.; Lee, Y.; Zhang, Y.; Stellacci, F.; Nazeeruddin, M. K.; Gao, P. From Nano-to Micrometer Scale: the Role of Antisolvent Treatment on High Performance Perovskite Solar Cells. *Chem. Mater.* **2017**, *29*, 3490–3498.
- (23) Jeon, N. J.; Noh, J. H.; Kim, Y. C.; Yang, W. S.; Ryu, S.; Seok, S. I. Solvent Engineering for High-Performance Inorganic–Organic Hybrid Perovskite Solar Cells. *Nat. Mater.* **2014**, *13*, 897–903.
- (24) Yang, W. S.; Noh, J. H.; Jeon, N. J.; Kim, Y. C.; Ryu, S.; Seo, J.; Seok, S. I. High- Performance Photovoltaic Perovskite Layers Fabricated through Intramolecular Exchange. *Science* **2015**, *348*, 1234–1237.
- (25) Zhou, Y.; Game, O. S.; Pang, S.; Padture, N. P. Microstructures of Organometal Trihalide Perovskites for Solar Cells: their Evolution from Solutions and Characterization. *J. Phys. Chem. Lett.* **2015**, *6*, 4827–4839.
- (26) Bishop, J. E.; Mohamad, D. K.; Wong-Stringer, M.; Smith, A.; Lidzey, D. G. Spray- Cast Multilayer Perovskite Solar Cells with an Active-Area of 1.5 cm². *Sci. Rep.* **2017**, *7*, 7962.
- (27) Ulicna, S.; Dou, B.; Kim, D. H.; Zhu, K.; Walls, J. M.; Bowers, J. W.; van Hest, M. F. Scalable Deposition of High-Efficiency Perovskite Solar Cells by Spray-Coating. *ACS Applied Energy Materials* **2018**, *1*, 1853–1857.
- (28) Jacobsson, T. J.; Correa-Baena, J.-P.; Pazoki, M.; Saliba, M.; Schenk, K.; Grätzel, M.; Hagfeldt, A. Exploration of the Compositional Space for Mixed Lead Halogen Perovskites for High Efficiency Solar Cells. *Energy Environ. Sci.* **2016**, *9*, 1706–1724.
- (29) Baena, J. P. C.; Steier, L.; Tress, W.; Saliba, M.; Neutzner, S.; Matsui, T.; Giordano, F.; Jacobsson, T. J.; Kandada, A. R. S.; Zakeeruddin, S. M.; Petrozza, A.; Abate, A.; Nazeeruddin, M. K.; Grätzel, M.; Hagfeldt, A. Highly Efficient Planar Perovskite Solar Cells Through Band Alignment Engineering. *Energy Environ. Sci.* **2015**, *8*, 2928–2934.
- (30) Sanchez, S.; Hua, X.; Phung, N.; Steiner, U.; Abate, A. Flash Infrared Annealing for Antisolvent-Free Highly Efficient Perovskite Solar Cells. *Adv. Energy Mater.* **2018**, *8*, 1702915.
- (31) Abbas, G.; Assender, H.; Ibrahim, M.; Martin Taylor, D. Organic Thin-Film Transistors with Electron-Beam Cured and Flash Vacuum Deposited Polymeric Gate Dielectric. *J. Vac. Sci. Technol., B: Nanotechnol. Microelectron.: Mater., Process., Meas., Phenom.* **2011**, *29*, No. 052401.